Color-Coded Fiber-Optic Tactile Sensor for an Elastomeric Robot Skin

Zhanat Kappassov, *Member, IEEE*, Zharaskhan Kuanyshuly, Daulet Baimukashev, *Student Members, IEEE*, Yerzhan Massalin, Arshat Urazbayev and Huseyin Atakan Varol, *Senior Member, IEEE*

***Abstract*— The sense of touch is essential for reliable mapping between the environment and a robot which interacts physically with objects. Presumably, an artificial tactile skin would facilitate safe interaction of the robots with the environment. In this work, we present our color-coded tactile sensor, incorporating plastic optical fibers (POF), transparent silicone rubber and an off-the-shelf color camera. Processing electronics are placed away from the sensing surface to make the sensor robust to harsh environments. Contact localization is possible thanks to the lower number of light sources compared to the number of camera POFs. Classical machine learning techniques and the state-of-the-art deep learning were used for contact localization. Specifically, we generated the mapping from stimulation to sensation of a robotic perception system using our sensor. We achieved a force sensing range up to 25 N with the force resolution of around 0.5 N and the spatial resolution of 5 mm. The color-coded tactile sensor is suitable for tactile exploration and might enable further innovations in robust tactile sensing.**

I. Introduction

Somatosensory system is responsible for human sensations through the skin. It can be considered the hidden ingredient of human dexterity in object manipulation. With the robots replacing humans in more and more tasks, tactile sensing is also becoming essential for robots. This sense provides a direct one-to-one mapping of the object's shape to the acquired signals [1]. Such mapping is necessary for dexterous manipulation and for safe human-robot interaction (HRI) [2]. Development of robust and effective tactile sensors is a major challenge that could lead to advances in the safety, responsivity, and dexterity of robots [3].

While sensing capabilities of the tactile sensors are improving [4], there is also a need for qualitative improvements – the sensors should be abrasion and water resistant – as robots move from industrial workcells into human-inhabited environments [5]. In human environments, a robot should be able to manipulate an object with liquids in it [6] or do it immersed inside water [7]. Since water is an electroconductive media, a robust sealing is necessary to keep the electronic processing units safe. Sealing requires continuous maintenance as well as complex manufacturing and assembling for robot fingertips [8]. This can be mitigated by placing fragile signal processing electronics away from the sensing unit, that is attached onto the fingertips. Such implementation would also allow a humanoid robot to have a centralized processing unit, e.g. in its torso.

We address this problem by developing an optical tactile sensing array, which uses physical interaction with an object to provide force sensing and contact localization. We deliver the light from three sources with different colors to a commodity vision camera via plastic optical fibers (POFs) embedded in transparent silicone. We use this compressible silicone as a color-coded tactile sensor (see Fig. 1). This tactile sensor is energy efficient thanks to the use of less number of light sources than the camera POFs. Moreover, working with light beams rather than with a flow of electrons can have advantages for some applications. For instance, data flow through electrical cables can be distorted by a magnetic field, but magnetic fields do not interfere with optical signals [9].

In the remainder of this paper, we firstly review the related work in Sec. II. In Section III, we explain the working principle and software development of our color-coded tactile sensor, and then we introduce its fabrication process in Sec. IV. Afterward, we present our experimental results on force measurement and contact localization to assess the performance of our sensor (see Sec. V). For these measurements, we use machine learning methods to measure the contact force from the previously acquired samples (see Sec. V-C). The last section summarizes our work.

II. Related work

Several types of tactile sensors based on various transduction methods (e.g. capacitive, resistive, magnetic, and optical) were reviewed in [3]. Optical sensing has high spatial resolution, sensitivity, repeatability and also immunity from electromagnetic interference. Moreover, some of these optical sensors can work under high ambient pressures (up

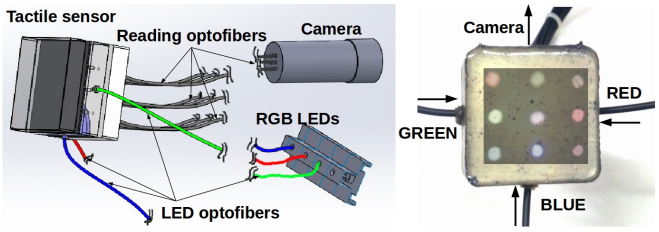

Fig. 1: Color-coded tactile sensor. (a) Assembly with LEDs, camera and plastic optical fibers. (b) Camera snapshot overlaid onto the sensor. The camera image is processed to infer sensor deformation.

This work was partially supported by the Ministry of Education and Science of the Republic of Kazakhstan grant "Methods for Safe Human Robot Interaction with Variable Impedance Actuated Robots" and Nazarbayev University internal grant "Robotic Artificial Tactile Perception".

Z. Kappassov, Z. Kuanyshuly, D. Baimukashev, Y. Massalin, A. Urazbayev and H. A. Varol are with the Dept. of Robotics and Mechatronics, Nazarbayev University, 53 Kabanbay Batyr Ave, Z05H0P9 Astana, Kazakhstan. Email: {zhkappassov, zharaskhan.kuanyshuly, dbaimukashev, yerzhan.massalin, aurazbayev, ahvarol}@nu.edu.kz.

Corresponding author: Z. Kappassov.

TABLE I: Raw Materials Used in Tactile Sensing via Optical Transduction

Material	Disadvantages	Advantages	Applications
Silicone (®*Smooth-on Sorta Clear18*)	-	Robustness, biocompatibility	Molding, food production
Silicone (®*Techsil RTV27905*)	-	Robustness, light propagation properties	Encapsulation and protection of electronics
Thermoplastic elastomer [10]	-	High spatial resolution	Injection molding
Polyurethane	-	Robustness	Car tires
Hydrogels[11]	-	Elasticity, durability	Biosensing
Plastic opto-fibers [12]	Not elastic	-	Communication
Polyethylene foam [13]	-	-	Packaging, filtering
Stereolithography resin (®*Formlabs*)	Not durable	-	Rapid prototyping
Stretchable fibers [14]	-	-	Medical textiles

to 600 bar) [13]. Next, we first summarize the materials for these optical tactile sensors and then overview the existing sensors.

A. Materials

There are different types of materials which are used for optical sensing: various polymers including silicone, polyurethane, and thermoplastic elastomers; POFs and hydrogels (see Table I).

Liquid silicone rubber compounds (e.g. ®Smooth-on Sorta Clear 18 and ®Techsil RTV27905) are widely used in injection molding to create robust parts. The part quality mainly depends on how well the silicone compounds are mixed during molding. On the other hand, thermoplastic rubbers, as in [10], provide a better ability to return to their original shape after stretching them to moderate elongations. These can be processed by heating the granules of thermoplastic elastomer, shaping them under pressure, and then cooling them to solidify. In contrast to silicone rubber and elastomers, polyurethanes can be synthesized by chemical reactions. Polyurethane parts are durable to tear and wear.

Molding the above-mentioned materials requires manufacturing steps that can be avoided by 3D-printing. Stereolithography resin, e.g. ®Formlabs or ®Objet, can be used for rapid prototyping. However, these parts still lack the durability and strength of the classical counterparts.

In order to make manufactured parts wearable and biocompatible, technological advances in bioengineering led to the emergence of hydrogels [11]. A hydrogel, a rubbery and transparent material composed mostly of water, can also be a good choice for safe physical HRI.

Robot sensing technology can also leverage advances in telecommunications besides the ones in bioengineering. Glass and plastic fibers can be used as force sensors [12]. Stretchable fibers [14] that respond to deformations with a color variation can measure strain forces. Tactile sensing using such stretchable fibers is accomplished by periodically changing the refractive index along the length of a fiber.

B. Optical Sensors

Using the materials in Sec II-A, a variety of optical tactile sensors were presented in the robotics literature (see Table II). The general principle is based on the optical reflection between mediums with different refractive indices. A conventional optical tactile sensor consists of an array of infrared light-emitting diodes (LEDs) and photodetectors. The intensity of the light is usually proportional to the magnitude of the pressure [12]. GelSight [10] tactile sensor uses a thermoplastic elastomer coated with a reflective membrane to capture surface textures with a camera. In [18], this sensor was benchmarked in texture recognition problem. Similarly, Nathan's group at the University of Bristol has developed a family of optical tactile sensors that are almost ready for small-scale mass production [4]. Their TacTip sensor uses a commodity image tracker originally for use in optical computer mice. It combines an image acquisition system and a digital signal processor, capable of processing the images at 2000 Hz [19]. Thanks to the high image processing rate, they can detect the slippage of a grasped object [20]. In [15], a touch sensor, consisting of 41 silicone rubber markers, a light source, and a camera, estimates tangential and normal forces by tracking these markers. Markers with different colors are used in GelForce [17] sensor.

Another optical tactile sensor is embedded into the multimodal tactile sensing system of an underwater robot gripper [13]. As in [9] and ®Optoforce sensor, the sensing principle is based on the light reflection delivered via POFs. The POFs can be used as force sensing elements due to the stray light, which is considered as a drawback in telecommunications [12]. A deformation of a POF increases losses of the light propagated inside, as the attenuation coefficient increases. However, besides the attenuation coefficient, elasto-optic metamaterial [14], can change its refractive index due to pure bending. Such POFs are fabricated by the chemical vapor deposition technique. Their design relies upon optical interference [21] that produces different colors.

Laboratory prototypes of image-based tactile sensors were reported in [16] and [17]. In these sensing panels, LEDs and photo-diodes/camera were placed against a reflecting planar surface. When the surface deforms, it causes changes in reflected beams. These sensors use optical light to detect deformation of the contact surface, which can be used to estimate the force.

In contrast to the mentioned above approaches, we aim in keeping the processing and conditioning electronics away from the touch sensing matter to increase the durability. In order to estimate both the contact force and its location, we

TABLE II: Tactile Sensors Based on Optical Transduction Technology

Sensor	# of Sources	# of Taxels	Res.	Advantages	Disadvantages
GelSight [10]	1 RGB LED ring	1 camera	$\sim 1\mu m$	High res. of contact deformation	Surface delamination, not water resistant
TacTip [4]	1 white LED ring	$\sim$200	$<1mm$	3D fingertip-like shape	Surface delamination
Plastic Opto-fibers [12]	6 white LEDs	6 Photo- resistors	$\sim 10mm$	Simplicity	Repeatability, ambient light dependent
Foam [13]	36	36 and 1 camera	$\sim 15mm$	Water resistant, remote connection	# light sources = # taxels
Three-axis sensor [15]	1 white LED	41 and 1 camera	$\sim 10mm$	Shear force sensing	Size
Mirror-based sensor [9]	9 white LEDs	9 with 1 camera	$>10mm$	Remote connection	Not stretchable
Elastic bandage [14]	Thorlabs SLS201	Spectro- meter	-	Stretchable	Contact localization
Touch panel [16]	White LEDs	Chess pattern and 1 camera	-	-	-
GelForce [17]	White LEDs	48 markers and 1 camera	2.5 mm	-	-
®Optoforce sensor	-	-	-	Force and torque sensing. Robust.	One contact point

feed the sensor with three different colors. Our solution is covered in the next section..

III. Color-Coded Sensor Design

We tackled the issues in the manufacturing and signal conditioning, that the current sensors share to some extent, using off-the-shelf items. To enable force measurements, a commodity camera records the light intensity of POFs embedded in a layer of silicone (Smooth-On Sorta Clear 18) (see Fig. 2a). Transparent silicone is widely used in molding applications. It does not require complex manufacturing, while satisfying the transparency and mechanical requirements such as water and abrasion resistance [22]. In the following, we first describe the sensing principle using such silicone with a commodity camera and then describe our sensor fabrication process.

A. Sensing Principle

When red, green and blue light frequency bands are mixed together, white color appears. If one of these bands is excluded, another color is observed, e.g. cyan when the red band is excluded. Figure 2b illustrates this principle. When the red color band is excluded, its intensity is zero. However, if its intensity is slightly lowered, then the resulting color would be different than white. The color changes can be detected by acquiring the color data using a RGB camera. When mixed in some soft and transparent matter, these color changes might be used to measure material deformations.

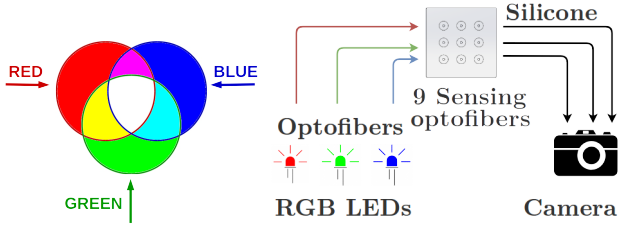

(a) (b)

Fig. 2: Sensing principle (a) and block diagram (b) of our tactile sensor.

We choose a transparent silicone as the light propagation medium. This silicone is supplied by three light emitting diodes (LEDs) with different colors. Plastic optical fibers deliver this light into the silicone material and also deliver the emerging color within this matter to a commodity red-green-blue (RGB) vision sensor. Figure 2b exemplifies the block-diagram of such connection with the transparent silicone as a color-coded sensor. We utilize 12 POFs: three of these POFs emit light into the silicone. The emitted light is scattered inside silicone and is received by the rest nine POFs.

As soon as the silicone gets compressed due to contact with an object, the light scattering pattern changes. Thus, the silicone rubber serves as a continuous pressure sensor – if its color changes, one can use the color chart to determine whether and to what depth the silicone is deformed. Thus, the color-coded silicone substrate acts as a pressure-sensing media and changes color to signal pressure level. Figure 3a shows the general principle and exemplifies a single point-contact. We denominate the locations of the POFs guiding the reflected light from the silicone to a camera as the tactels. During the deformation of the sensing surface under an external force, some of the tactels get more light than others and vice versa as the directions of the reflected light beams change. The reflection is realized using a thin film. Figure 3b illustrates these tactels, i.e. locations of the nine receiving POFs.

Since the silicone substrate can be approximated by a spring with a constant Youngs modulus E, then the force as function of deformation d is given by

$$F \propto \frac{EA}{D}\, d, \tag{1}$$

where A is the contact area over the sensor and D is the thickness of the silicone rubber.

Let the emitted light intensity be I_0 and the measured reflected intensity from an object be I. Depending on the index of refraction of the rubber material, a fraction k will be scattered, and a fraction α will be reflected at the target surface. After the contact with an object, the silicone gets compressed by $d \propto \Delta F / EA$, leading to the following relation

between the reflected light intensity and the contact force:

$$I \propto I_0 \frac{\alpha}{(D - \frac{\Delta F}{EA})^2} - kI_0. \quad (2)$$

Equation (2) depends on the surface reflectance α of the thin film, which needs to be known for accurate force measurements. Moreover, the compression of the silicone eventually alters the scattering and absorption properties, which dramatically increase for large deformations. For example, the LED light intensity decreases due to increase of the density of irregularities. This effect depends on many properties, to name a few of them, the chemical composition and impurities, the details of which are beyond the scope of this paper. However, we should note that I_0 is heavily affected by absorption when the silicone is largely compressed. Bouguer's Law $I_0 \propto I_{led} exp(-\beta x)$ captures this relationship, where I_{led} is the light intensity of one LED, x is the path through which the photons from the LED travel, and β is the linear absorption coefficient (a characteristic of a particular material). Figure 3c exemplifies the increase of β due to the large compression of injected particles that block the LED light beams.

B. Raw Data Descriptor

In this subsection, we explain the image processing for our sensor. Since the received signals are light intensities; the change of red, green, and blue channel intensities of each reflected fiber can be used as a descriptor to infer both the force applied to the sensor array and the location of the contact. The descriptor algorithm is implemented using Robot Operating System (ROS) and OpenCV library. First, we acquire the images in real-time at 30 Hz. Then for each image, we define the regions of interest (ROI), R, around the locations of every POF. Hence, in the input images, there are nine rectangular ROIs $R_i,\ i = 1,2...9 \in Z_{\geq 0}^{w \times h}$, where w and h are the ROI width and height, respectively. We compute the mean values $\mu_j,\ j = 1,2...27$ of each region in the red, green and blue channels. As a result, we get nine mean values for each channel resulting in 27 features representing surface deformations. Using the resultant feature vector $s = (\mu_1, \mu_2, \mu_3, ..., \mu_{26}, \mu_{27}) \in R^{27}$, we infer the sensing surface deformation as described in Sec. V-C. Any surface deformation depends on the sensor material and fabrication which is described in the following section.

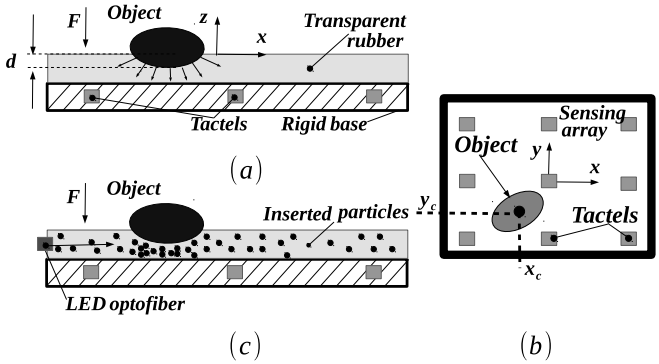

Fig. 3: Change of color in our color-coded tactile sensor. (a) Depending on an external force, the silicone deforms and the colors acquired by the camera via POFs changes. (b) Locations of nine POFs. (b) The light absorption coefficient changes as the silicone deforms.

IV. Fabrication

Eventually, we aim to attach color-coded tactile sensor to robot grippers for object manipulation. Therefore, the size of our sensor is $40 \times 40 \times 25$ mm. There are three fiber connections from the sides and nine fiber connections from the bottom. Figure 4 illustrates the fabricated sensor with these attached POFs. The distance between two neighboring POFs at the bottom side is 5 mm in both directions. The fibers that are on the sides are place to the center of the corresponding edges. The depth of the inserted fibers is 5 mm. There are also extruded adapter sockets for the POFs. These sockets with the height of 8 mm increase the robustness of the connection between the POFs and silicone. The shape of the sensor is obtained by molding silicone into a plastic mold. The mold is 3D-printed using PLA filament. The structure of the sensor includes three layers: silicone with injected light scattering particles, reflective thin film, and silicone with injected reflecting particles for durability and better light reflection.

A. Silicone Sensor Layers

1) Silicone Compound With Injected Powder Particles: The silicone is used both as the light transmission media and as a protective layer. There are different types of silicone compounds with different shore durometers [23]. The duruometer scale determines the hardness of elastic materials. For our tactile sensor, we used Sorta Clear silicone compound with shore level 18 from Smooth-On. We chose this material over the commonly used Polydimethylsiloxane (PDMS), e.g. as used in [22], due to its better elasticity

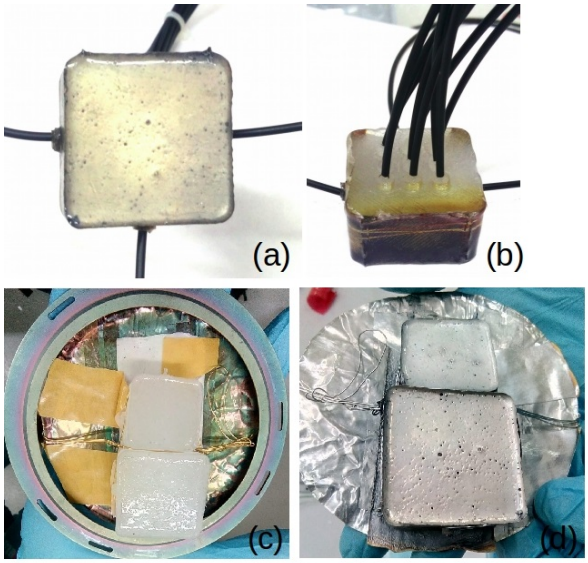

Fig. 4: Color-coded tactile sensor: (a) Front view of the sensor with silver thin film. (b) Entrance of the optofibers and their sockets into the sensor. (c) Silicone without thin film. (d) Silicone with silver thin film.

and durability. This allows large sensor surface deformations without sustaining damage [24].

The silicone is first poured into a mold. Then, the mold is placed inside a vacuum chamber for degassing. The proportion of the silicone components (part A and part B) is 10 to 1 and the solidification time is 24 hours. In this mold, we also add light scattering micro-scale powder particles, the effect of which is illustrated in Fig. 3c. After the molded silicone cures, it is covered with a reflective thin film.

2) Thin Film Magnetron Physical Vapor Deposition: The effect of a thin film reflective layer is exemplified in Fig. 4a. Figures 4c and 4d illustrate a silicone sample before and after adding the thin film. We tried several materials including Aluminum (Al), Copper (Cu) and Silver (Ag) for making this thin film. For Al target, the obtained thin film was black (probably due to the fast oxidization). The reflectance characteristics of Cu was not desirable. Ag worked best for our purposes without the oxidization problem.

To create this thin film, we used magnetron physical vapor deposition technique. We installed the silicone sample in front of the Ag electrode and pumped the chamber during in 90 min up to a pressure of 10^{-5} mT. The deposition of the Ag thin films on top of the silicone sensors is done by the magnetron sputtering at room temperature for eight minutes at 100 W. When the power is applied to the Ag electrode, the electrons accelerate in an electromagnetic field and applied voltage ionizes the Ar gas. This leads to the formation of the plasma ring on the surface of the Ag electrode, which sputters the Ag atoms from the electrode and results in the formation of the Ag film on the surface of the silicone sensor.

3) Protective Layer: The coated thin film wears and tears during physical contact with the environment. Therefore, we added one more silicone layer: Smooth On Sorta clear 18 mixed with a nickel powder. The nickel powder [1] is added to increase the reflectance of the thin film as the surface of the silicone is not perfectly flat (see Fig. 4).

B. System Integration

The deformation of the sensor illuminated from the side via three plastic POFs is captured from the bottom by a commodity camera via nine more POFs as shown in Fig. 5.

1) Light Sources: We obtain red, green, blue light sources by use of corresponding color filters and high power surface-mount LEDs (Nichia NVSW219CT). These LEDs are soldered on a metal-core printed circuit board (MCPCB), and are driven with 200 mA current to obtain the luminous flux of 250 lm. A color filter is placed onto each LED (fixed by a custom 3D-printed adapter, which is also used as a clamp for the POFs as shown in Fig. 5a). Figure 5c illustrates how these clamps are placed on the MCPCB. There are 16 LEDs on it, but we only use three.

2) Optofibers: In order to prevent stray light, we used TLC 1 mm Simplex Plastic Fiber (Part Number: P96TB01TRBL22), which is covered with an insulation layer. Diameter of the core is 1 mm, and the external diameter with the insulation layer is 2.2 mm. Glue is used to fix the fibers to the LED clamps (see Fig. 5a). In order to avoid a drop of the light intensity, the ends of the fibers were polished using a rotary tool (Dremel 4300) with fine sandpaper.

3) Camera: The light beams from POFs are acquired to a desktop computer (Intel Xeon E5620, 4 GB DDR3 memory, Ubuntu 16.04 Linux operating system) using an off-the-shelf camera (Logitech HD Pro Webcam C920) at 30 Hz. Data is sent via Robot Operating System (ROS) environment at 30 Hz using *libuvc* library. We replaced the lens of the camera with a macro-lens (2 cm focus length) due to the short distance between the sensing POFs and the camera. POFs are fixed so that the ends of them are facing the camera lens vertically (see Fig. 5b).

V. Sensor Characterization

The fabricated sensor measures the contact force applied to its sensing surface. This contact force can be inferred from the changes in the camera image. Therefore, we need the relation between the applied force and ROI mean values for each color channel. We find this relation by compressing our tactile sensor using a robot arm equipped with a ground-truth force sensor. Exact relation between the applied force and changes in camera images depends on a variety of fabrication properties, the details of which are beyond the scope of this paper. More details can be found in [25] for light propagation and in [23] for mechanical properties of silicone materials.

A. Platform and Experimental Scenario

We characterized the fabricated sensor using an industrial robot. The UR10 robot (Universal Robots) was controlled using the Position/Velocity command interface running at 125 Hz. Ground-truth force measurements were obtained by a force/torque sensor (Weiss KMS 40) attached to the robot's end-effector. The arm controller and the force sensor interfaces were both implemented using ROS. An indentor [23] was attached on the ground-truth force sensor to compress the tactile sensor at exact locations. The indentor has a dome-shape with 2 mm tip radius. Figure 6 shows this setup.

The robot end-effector moved vertically to press the color-coded tactile sensor, which was placed inside a 3D-printed plastic box and fixed on an optical table. First, we fond

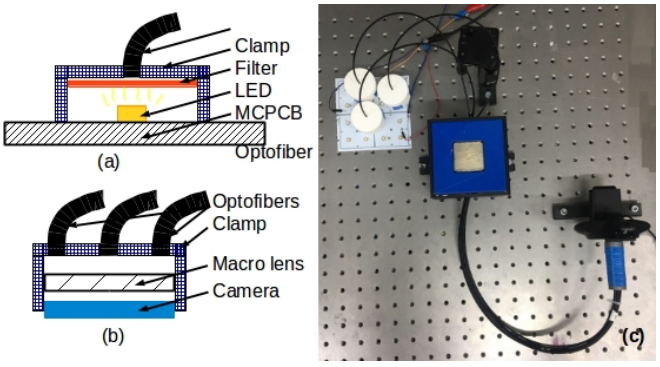

Fig. 5: Clamps: (a) Clamping structure for an LED, color filter and POF, (b) clamping structure for the camera with the macro lens and POFs. (c) System integration.

[1]Nickel Silver Powder Smooth-On(c) https://www.smooth-on.com/products/nickel-silver-metal-powder/

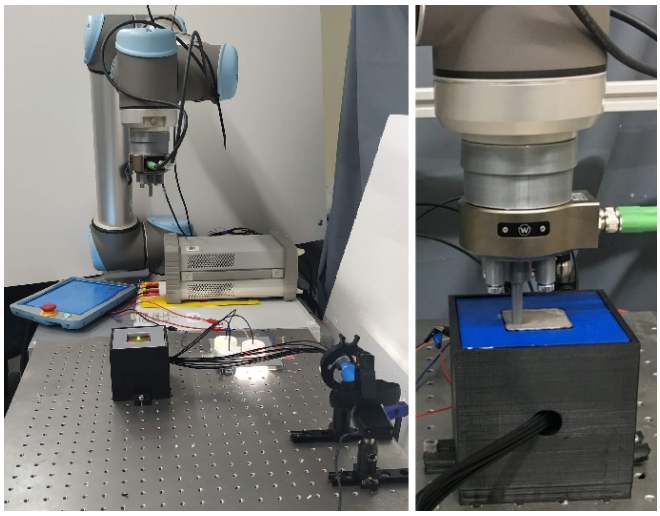

Fig. 6: Calibration setup consisting of the UR10 robot arm (Universal Robots) and Weiss Robotics force sensor with the attached indentor (left). The indentor pressing down on the silicone sensor (right).

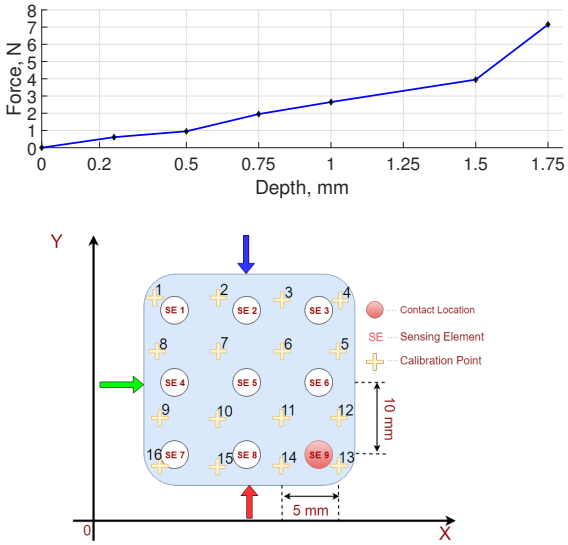

Fig. 7: (a) Force versus depth plot for up to 8 N, and (b) the locations of contacts and optofibers.

the end-effector pose when the indentor was at the closest proximity to the sensor without registering any force. Then, the end-effector progressively squeezed the tactile sensor up to 8 mm with 1 mm steps (i.e. 8 depth levels). Afterward, the robot end-effector moved back until to the pre-touch position, positioned itself to a new location to squeeze the sensor again. There were 16 total locations, and therefore, 16×8 contact states. We recorded 250 images at each contact state.

B. Surface Deformation and Force

The thickness of the silicone dictates the maximum allowable displacement range and, thereby, the maximum measurement force and its resolution [22]. In our sensor design, we achieved the maximum detectable displacement range of 8 mm. Figure 7 shows the response of the fabricated molded silicone up to this displacement. This rather large displacement range would allow a robotic system to maintain robust contacts [26]. However, there is a trade-off between the maximum displacement range and the sensitivity. Therefore, 4 N of applied force causes only 1 mm of displacement from the resting state.

Force values and depth of the deformations exemplified in Fig. 7a were obtained by squeezing the silicone at 16 locations. The locations of these contacts and the POFs are illustrated in Fig. 7b. By applying (1) to the measurements, we get the Young's modulus of our sensor as 0.0059 GPa.

C. Estimation of Surface Deformation From the Image

As described in Sec. III-B, we obtain the feature vector s by computing the mean values of ROIs. In order to validate this, we computed the sum of this feature vector as

$$s_{\in} = \sum_{i=1}^{27} s_i \tag{3}$$

TABLE III: Image-to-force classification results

Method	Cross Validation Accuracy %
LDA	93.6
QDA	99.8
Linear SVM	96.2
Cubic SVM	99.9
Quadratic SVM	99.8
$k-$nn	99.9

and plotted it versus the surface deformation depths. Figure 8 shows $s_{\in}$ for two different locations and four different depth levels. The sum of the feature vector is a raw estimate of the surface deformation.

The optical response of the sensor, i.e. $s_{\in}$, is not the same for every contact location: curvatures have different shapes. For instance, when the indentor squeezes our sensor at location 1, $s_{\in}$ decreases, whereas at location 5 it increases with the depth of the penetration. Thus, a machine learning technique would be suitable to build the map from stimulation to sensation of a robotic perception system.

D. Image-to-Force Map

Various classification approaches can be applied to infer the contact information including the force [19], [10]. We applied traditional machine learning approaches such as Support Vector Machines (SVM), $k-$nearest neighbors ($k-$nn), Linear Discriminant Analysis (LDA), and Quadratic Discriminant Analysis (QDA). Table III outlines cross validation accuracies of these methods. In order to obtain the results, we collected 250 trials per class and allocated 200 of these for training and 50 for testing. Number of classes is 128 due to 16 contact point locations and 8 depth levels of the indentor (see Fig. 7b).

The classification methods have a high accuracy. Among these methods, QDA classifier with 99.8% of accuracy

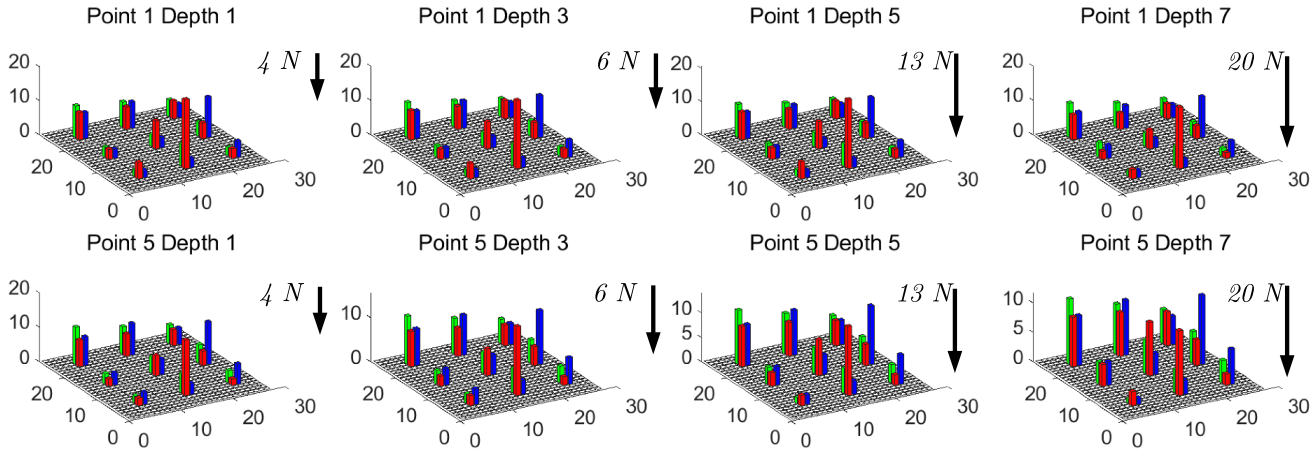

Fig. 8: 3D surface visualization by feature vectors at different contact locations and depths: 1 mm (first column), (b) 3 mm (second column), (c) 5 (third column), and (d) 7 mm (fourth column). Each feature vector corresponds to the applied contact force at a given contact location.

requires less memory and computational time. The results can be better interpreted by projecting the feature vectors (s), representing 128 classes, into two-dimensional space (see Fig. 9). Every color in the figure represents a separate class. In the 2D-projection (see Fig. 9), we see that the feature vectors are separated into separate classes. The generalization accuracy on the testing data also reaches 99.7%.

E. CNNs to Decipher the Image-to-Force Map

Inspired by the biological nature of the sensing cortex, we applied neural networks and showed that the same results can be obtained even without the descriptor explained in Sec. III-B. State-of-the-art deep Convolutional Neural Network (CNN) architecture was utilized. By training the network, we find a set of weights and biases which minimizes the loss function. Resulting trained deep network can then be used to predict contact location and depth of the surface deformation for new samples (i.e. camera images).

The CNN topology with two convolutional and two fully-connected layers is depicted in Fig. 10. The final layer has the size of 128, which is the number of contact states in the experimental scenario described in Sec. V-A). This layer represents the result of classification. We apply 64 convolutions with the size of 80x80 in the first layer and set the learning rate 0.1. With these parameters, our topology achieves 100% training and 99.42% validation accuracy at the sixth epoch.

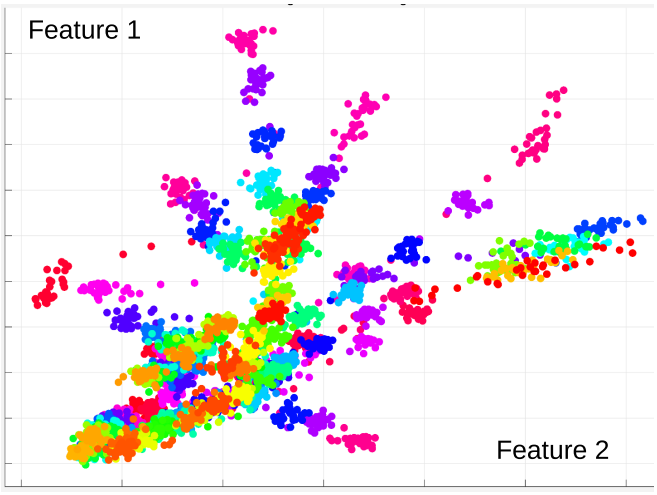

Fig. 9: Projection of feature vectors into 2D space using the first two features as basis vectors.

VI. Conclusion

In this work, we presented the design and implementation of our POF-based tactile sensor prototype. Our approach combines known optical design concepts with soft materials and utilizes three different colors to increase spatial resolution. The sensor acts as a force-sensing media – as its sensing surface deforms, the color acquired by the optical fibers change. Such sensor provides several benefits that normally involve more complex designs (e.g. robustness and durability). We evaluate the design idea experimentally and benchmark the efficacy of our sensor using a machine learning-based approach, in which we compare real and predicted sensor responses to different surface deformations. Experimental results confirm that the color-coded tactile sensor is able to infer contact forces and their locations. Thus, our sensor has the potential to improve the dexterity of various robots in physical interaction tasks. In the future, we will improve our sensor design (by optimizing design parameters) and also utilize it for tactile motion control (e.g. squeezing an object for determining its deformability).

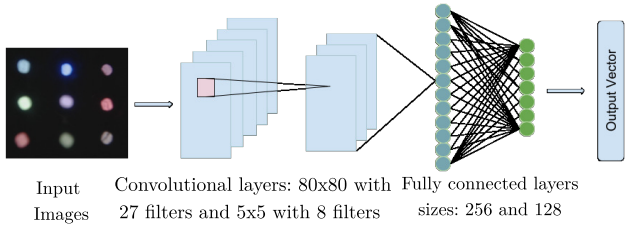

Fig. 10: CNN model with two convolutional and two fully-connected layers.

REFERENCES

[1] A. V. Terekhov and V. Hayward, "The brain uses extrasomatic information to estimate limb displacement," *Proceedings of the Royal Society of London B: Biological Sciences*, vol. 282, no. 1814, 2015.

[2] B. Navarro, *et al.*, "In pursuit of safety: An open-source library for physical human-robot interaction," *IEEE Robotics Automation Magazine*, vol. 25, no. 2, pp. 39–50, June 2018.

[3] Z. Kappassov, J.-A. Corrales, and V. Perdereau, "Tactile sensing in dexterous robot hands: Review," *Robotics and Autonomous Systems*, vol. 74, pp. 195 – 220, 2015.

[4] B. Ward-Cherrier, *et al.*, "The TacTip Family: Soft optical tactile sensors with 3D-printed biomimetic morphologies," *Soft Robotics*, vol. 5, no. 2, pp. 216–227, 2018.

[5] B. Gates, "A robot in every home," *Scientific American*, vol. 296, no. 1, pp. 58–65, 2007.

[6] C. Schenck and D. Fox, "Perceiving and reasoning about liquids using fully convolutional networks," *The International Journal of Robotics Research*, vol. 37, no. 4-5, pp. 452–471, 2018.

[7] H. Stuart, *et al.*, "The ocean one hands: An adaptive design for robust marine manipulation," *The International Journal of Robotics Research*, vol. 36, no. 2, pp. 150–166, 2017.

[8] P. Kampmann and F. Kirchner, "Towards a fine-manipulation system with tactile feedback for deep-sea environments," *Robotics and Autonomous Systems*, vol. 67, pp. 115 – 121, May 2015.

[9] H. Xie, *et al.*, "Magnetic resonance-compatible tactile force sensor using fiber optics and vision sensor," *IEEE Sensors Journal*, vol. 14, no. 3, pp. 829–838, Mar 2014.

[10] W. Yuan, S. Dong, and E. H. Adelson, "Gelsight: High-resolution robot tactile sensors for estimating geometry and force," *Sensors*, vol. 17, no. 12, 2017.

[11] K. Gawel, *et al.*, "Responsive hydrogels for label-free signal transduction within biosensors," *Sensors*, vol. 10, pp. 4381–4409, 2010.

[12] D. Sartiano and S. Sales, "Low cost plastic optical fiber pressure sensor embedded in mattress for vital signal monitoring," *Sensors*, vol. 17, no. 12, 2017.

[13] P. Kampmann and F. Kirchner, "Integration of fiber-optic sensor arrays into a multi-modal tactile sensor processing system for robotic end-effectors," *Sensors*, vol. 14, no. 4, pp. 6854–6876, 2014.

[14] J. D. Sandt, *et al.*, "Stretchable optomechanical fiber sensors for pressure determination in compressive medical textiles," *Advanced Healthcare Materials*, p. 1800293, Aug 2018.

[15] M. Ohka, *et al.*, "Object exploration and manipulation using a robotic finger equipped with an optical three-axis tactile sensor," *Robotica*, vol. 27, no. 5, pp. 763–770, 2009.

[16] S. Saga, R. Taira, and K. Deguchi, "Precise shape reconstruction by active pattern in total-internal-reflection-based tactile sensor," *IEEE Transactions on Haptics*, vol. 7, no. 1, pp. 67–77, Jan 2014.

[17] K. Sato, *et al.*, "Finger-shaped gelforce: Sensor for measuring surface traction fields for robotic hand," *IEEE Transactions on Haptics*, vol. 3, no. 1, pp. 37–47, Jan 2010.

[18] S. Luo, *et al.*, "ViTac: Feature sharing between vision and tactile sensing for cloth texture recognition," *CoRR*, vol. abs/1802.07490, 2018.

[19] N. Pestell, *et al.*, "Dual-modal tactile perception and exploration," *IEEE Robotics and Automation Letters*, vol. 3, pp. 1033–1040, 2018.

[20] J. W. James, N. Pestell, and N. F. Lepora, "Slip detection with a biomimetic tactile sensor," *IEEE Robotics and Automation Letters*, vol. 3, no. 4, pp. 3340–3346, Oct 2018.

[21] K. Nagano, S. Kawakami, and S. Nishida, "Change of the refractive index in an optical fiber due to externalforces," *Applied Optics*, vol. 17, no. 13, pp. 2080–2085, Jul 1978.

[22] R. Patel, R. Cox, and N. Correll, "Integrated proximity, contact and force sensing using elastomer-embedded commodity proximity sensors," *Autonomous Robots*, Apr 2018.

[23] H. J. Qi, K. Joyce, and M. C. Boyce, "Durometer hardness and the stress-strain behavior of elastomeric materials," *Rubber Chemistry and Technology*, vol. 76, no. 2, pp. 419–435, 2003.

[24] C. H. King, *et al.*, "Optimization of a pneumatic balloon tactile display for robot-assisted surgery based on human perception," *IEEE Transactions on Biomedical Engineering*, vol. 55, no. 11, pp. 2593–2600, Nov 2008.

[25] Z. Cai, *et al.*, "A new fabrication method for all-PDMS waveguides," *Sensors and Actuators A: Physical*, vol. 204, pp. 44 – 47, 2013.

[26] Z. Kappassov, *et al.*, "A series elastic tactile sensing array for tactile exploration of deformable and rigid objects," in *Proc. of the IEEE/RSJ Int. Conf. on Intelligent Robots and Systems (IROS)*, 2018, (to appear).